Journal Name

ARTICLE

Selective Recognition of Biologically Important Anions Using an All-Conjugated Diblock Polyfluorene-Polythiophene Conjugated Polyelectrolyte

Received 00th January 20xx,
Accepted 00th January 20xx

DOI: 10.1039/x0xx00000x

www.rsc.org/

Niamh Willis-Fox,[a‡] Andrea Gutacker,[b‖] Michelle P. Browne[a], Amir R. Khan[c], Michael E. G. Lyons[a], Ullrich Scherf[b] and Rachel C. Evans[a,d*‡]

The all-conjugated diblock copolymer poly[9,9-bis(2-ethylhexyl)fluorene]-*b*-poly[3-(6-trimethylammoniumhexyl) thiophene] bromide (**PF2/6-*b*-P3TMAHT**) shows dual fluorescence from the polyfluorene (PF) and polythiophene (PT) blocks. Interaction with a range of nucleotide phosphates, at biologically relevant concentrations, was observed to bring about a dramatic quenching of the PT emission, leaving the PF emission unaffected. The magnitude of this ratiometric response was found to depend on the number of phosphates attached to the nucleotide (guanosine triphophate (**GTP**) > guanosine diphphosphate (**GDP**) > guanosine monophosphate (**GMP**)), the type of nucleobase and the concentration. Modelling of the quenching behaviour, along with electrochemical studies suggest a mechanism involving energy transfer from the PF block to the PT block followed by electron transfer from the PT to the nucleotides held in a Stern layer around the polymer core-shell aggregate that form in water. Notably, the ability to discriminate between different numbers of phosphate groups is extremely relevant for energy metabolism processes. The enhanced insight into the quenching mechanism unravelled through this study provides the tools required to design targeted sensor platforms capable of discriminating different species through consideration of the size, charge and redox potential of the analyte.

1. Introduction

Conjugated polyelectrolytes (CPEs) combine the excellent optoelectronic properties of conjugated polymers with enhanced aqueous solubility conferred to them by the charged groups present in their side chains.[1,2] This improved solubility makes them highly desirable as optical sensors for a range of biological systems,[3,4] with the ionic terminal groups additionally serving as analyte recognition sites.[5,6] This approach has been elegantly demonstrated for various large bioanalytes such as DNA,[7,8] proteins,[9] lipids[10] and enzymes.[11] Ionic polythiophenes have been developed for a wide range of biosensing platforms due to their excellent optical properties and the possibility for self-assembly.[12,13] Yao *et al.* recently reported a polythiophene (PT)-based CPE system for the detection of nucleotide phosphates *via* a colorimetric response brought about by changes in aggregation of the PT backbone arising from the presence of the specific phosphate.[14] Nucleotide phosphates are the smaller building blocks of large biological moieties such as DNA and are extremely important substrates in processes such as energy metabolism.[15] Previously, we and others have shown how the cationic homopolymer poly[3-(6-trimethylammoniumhexyl) thiophene] bromide (**P3TMAHT**) undergoes electrostatic assembly with smaller, oppositely-charged species such as halide ions[16] or surfactants,[17] which leads to a change in the conformation and photoluminescence (PL) properties of the PT.

The addition of a second, distinct block to the CPE chain in the form of an all-conjugated diblock copolymer may impart further sensitivity towards the polymer environment.[18,19] The chemically-distinct nature of the constituent segments of block copolyelectrolytes provides a unique platform for self-assembly into structures organised on the nanometre scale,[20] while the differing properties of each block may also introduce complementary optical properties.[21] The importance of conformation and aggregation state of diblock CPEs has previously been demonstrated using the polyfluorene-polythiophene (PF-PT) polyelectrolyte, poly[9,9-bis(2-ethylhexyl)fluorene]-*b*-poly[3-(6-trimethylammoniumhexyl) thiophene] bromide (**PF2/6-*b*-P3TMAHT**) (**Fig. 1a**) in methanol-water[22] and THF-water mixtures.[23,24] The shape of the aggregates formed, and thus the optical properties, were found to depend highly on the polarity of the solvent. The fact that electrostatic binding of oppositely-charged species to the PT block of this copolymer induces the subsequent change in its

[a] *School of Chemistry and CRANN, Trinity College Dublin, The University of Dublin, Dublin 2, Ireland.*
[b] *Macromolecular Chemistry Group (buwmacro) and Institute for Polymer Technology, Bergische Universität Wuppertal, Wuppertal, Germany.*
[c] *School of Biochemistry and Immunology, University of Dublin, Trinity College Dublin, The University of Dublin, Dublin 2, Ireland.*
[d] *Department of Materials Science and Metallurgy, University of Cambridge, Cambridge, CB3 0FS, UK. E-mail: rce26@cam.ac.uk*
‡ Current address (NWF): Institute for Manufacturing, Department of Engineering, University of Cambridge, Cambridge, CB3 0FS, UK.
‖ Current address (AG): Henkel KGaA, 40191, Düsseldorf, Germany.
†Electronic Supplementary Information (ESI) available: [Supplemental photoluminescence spectra, isothermal calorimetry data, Stern-Volmer analysis and electrochemical measurements]. See DOI: 10.1039/x0xx00000x

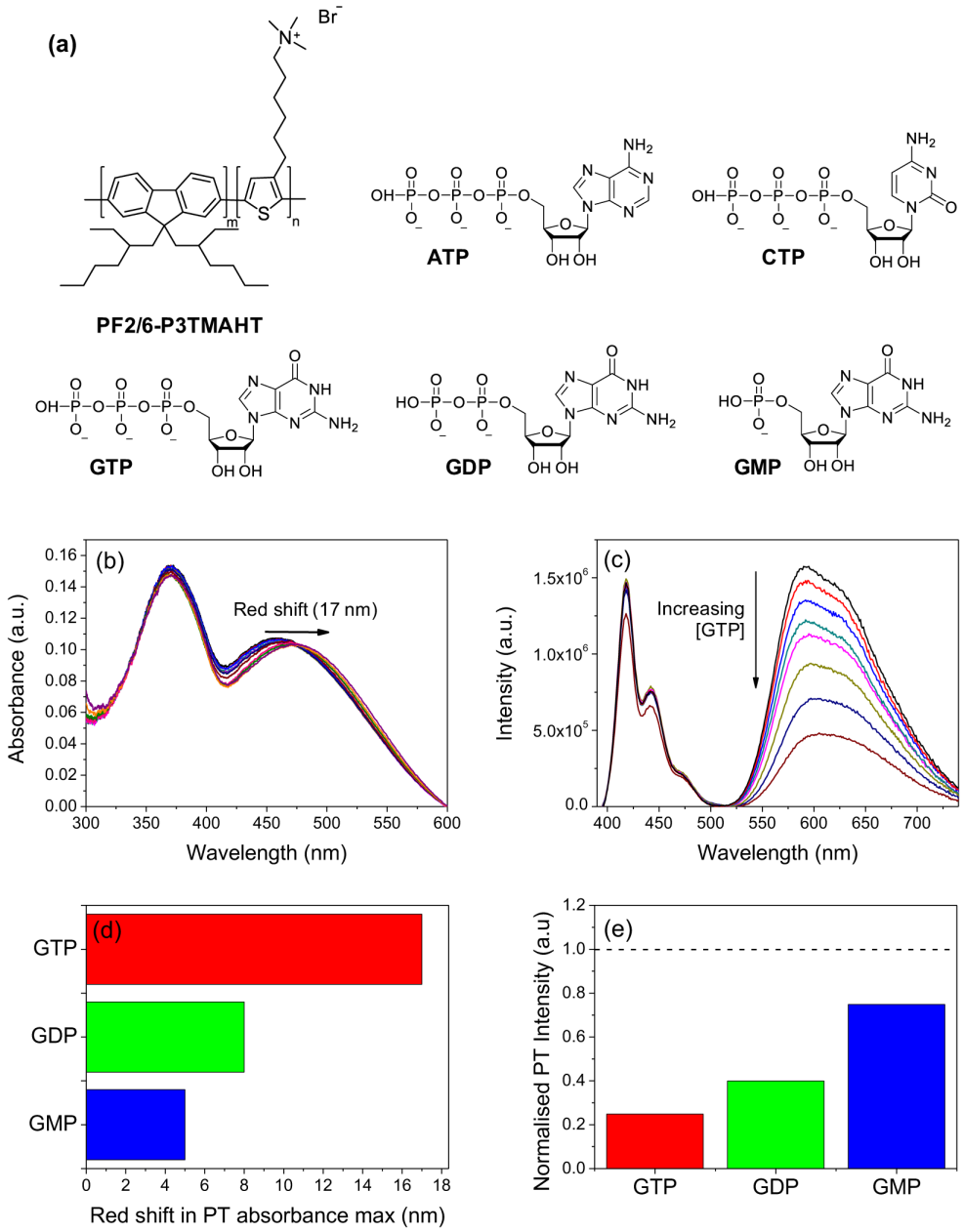

Figure 1. (**a**) Chemical structures of the CPE (**PF2/6-*b*-P3TMAHT**) and the bioanions used: adenosine triphosphate (**ATP**); cytidine triphosphate (**CTP**); guanosine triphosphate (**GTP**); guanosine diphosphate (**GDP**) and guanosine monophosphate (**GMP**). (**b**) UV/Vis absorption and (**c**) PL spectra (λ_{ex} = 380 nm) for **PF2/6-*b*-P3TMAHT** in aqueous solution in the presence of increasing concentration of **GTP** (0 – 38 μM). (**d**) Magnitude of the red-shift in the PT absorption maximum and (**e**) intensity of the PT emission on addition of an excess of **GTP**, **GDP** and **GMP,** normalised relative to the initial PT emission intensity. The black dash line serves only to guide the eye, indicating the relative intensity of the initial PT emission.

conformation and optical properties has allowed for the development of nucleobase fluorescence based sensors for both halide ions[16] and double- and single-stranded DNA.[16,25] The ratiometric nature of these sensing platforms results from the fact that ionic interactions between the analyte and pendent groups of the CPE block lead to selective quenching of the PT photoluminescence, while the emission of the non-complexed PF block remains unquenched.

Specific electrostatic interactions appear to play a significant role in the quenching of the PT block, suggesting that this diblock copolymer may potentially be developed as a platform sensory material for a host of anionic analytes. However, the specific mechanism for the PL quenching that drives the response of this system is still poorly understood.

To address this, here we report on the selective optical response of the all-conjugated diblock **PF2/6-P3TMAHT** in the presence of the biologically important nucleotide phosphates, guanosine triphosphate (**GTP**), guanosine diphosphate (**GDP**), guanosine monophosphate (**GMP**), adenosine triphosphate (**ATP**) and cytidine triphosphate (**CTP**) (**Fig. 1a**). These anions were chosen due to their important roles in RNA synthesis[26] and metabolic processes.[15] Nucleotide phosphates contain

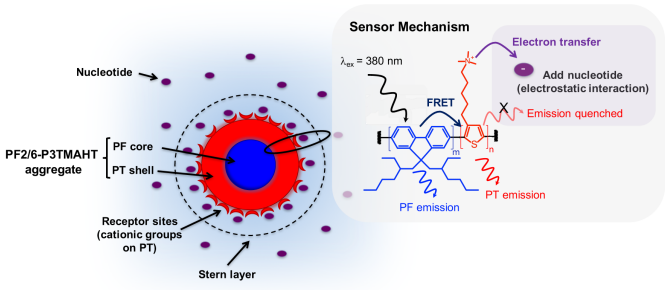

Scheme 1 Schematic representation of **PF2/6-*b*-P3TMAHT** (m = 37, n = 46) agggregates in water showing a PF rich core (blue) and PT shell (red) with the charged groups of the PT block acting as receptor sites on the aggregate surface. The sensor mechanism for the detection of nucleotides is also shown.

phosphate groups attached to a sugar which is attached to a nucleobase.[27] These nucleobases fall into two categories depending on their structure; purines and pyrimidines. Pyrimidine bases are six-membered heterocyclic aromatic rings containing two nitrogen atoms while purine bases consist of two fused heterocycles, a pyrimidine ring fused to an imidazole ring.[28]

Here, the optical properties of the CPE are examined as a function of the nucleobase, number of phosphate groups and concentration. We will unravel the mechanism behind the observed response *via* modelling of the quenching behaviour and investigation of the electrochemical properties. We anticipate that improved understanding of the mechanism behind the observed response should enable the targeted design of sensor platforms based on this simple motif to include a wide range of analytes.

2. Results and discussion

Optical Response

The absorption spectrum of **PF2/6-*b*-P3TMAHT** in aqueous solution shows two distinct bands (**Fig. 1b**) that arise as a superposition of the absorption bands of the individual blocks, with a maximum at 370 nm arising from the PF and a second at 460 nm attributed to the PT.[23] On direct excitation of the PF block (λ_{ex} = 380 nm), two bands are observed in the PL spectrum, attributed to the PF ($\lambda_{em,max}$ = 420 nm) and PT blocks ($\lambda_{em,max}$ = 630 nm), respectively (**Fig. 1c**). The observation of emission from the PT block following selective excitation of the PF block is attributed to Förster resonance energy transfer (FRET) from the PF to the PT block.[24] This is possible due to the excellent spectral overlap between the PF emission and PT absorbance (see ESI†, **Fig. S1a**). FRET is confirmed by the observation of a second band (associated with the PF block) in the PL excitation spectrum while monitoring at the PT emission maximum (see ESI†, **Fig. S1b**). As the FRET efficiency, and thus the observed optical properties are dependent on the molecular weight of each copolymer block, a single polymer sample was used throughout this study to ensure any observed response is due solely to the presence of the quencher species being examined. Previous studies on the solvent-driven aggregation of **PF2/6-*b*-P3TMAHT**[22] have shown that in water the polymer adopts a core-shell structure in which the hydrophobic PF block is predominantly contained in the aggregate core. The charged PT shell gives rise to the possibility of receptor-like sites for the anions through electrostatic interactions as highlighted in **Scheme 1**.

Addition of the nucleotides investigated in this study to an aqueous solution of **PF2/6-*b*-P3TMAHT** induces a response in both the UV/Vis absorption and PL spectra, the nature and magnitude of which are dependent on the nucleotide in question. The specific response seen on addition of **GTP** is shown in **Fig. 1b** and **1c**, as a representative example. Considering specifically the addition of the guanosine-containing nucleotides, a decrease in absorbance and a red-shift in the absorbance maximum of the PT block is observed, while the PF block is essentially unaffected. The magnitude of the shift in the PT absorption band is dependent on the number of phosphate groups on the anion following the trend **GTP>GDP>GMP**, as highlighted in **Fig. 1d**. The fact that the PF absorbance is unaffected suggests a unique binding interaction occurs between the nucleotide and the positively-charged PT units, as expected from the structure proposed in **Scheme 1.** Moreover, a red-shift such as that seen for the PT block indicates an increase in polymer aggregation upon binding.[29] While the corresponding PL spectra show little to no effect on the PF block, significant quenching of the PT emission occurs, the magnitude of which decreases as the number of phosphate groups on the anion decreases. The fact that the PF emission is essentially unaffected in the presence of the nucleotides gives rise to a ratiometric fluorescence sensor. The response in the presence of differing numbers of phosphates is highlighted in **Fig. 1e**, which shows the relative final emission intensity of the PT block compared to the initial emission intensity for addition of a large excess of **GTP**, **GDP** and **GMP**. The mechanism of action of these nucleotides within the cell during processes such as metabolism involves transfer of phosphoryl groups between substrates.[30] Thus, the ability to differentiate between the numbers of phosphate groups as seen here is of utmost importance. This particularly highlighted when considering the energy charge of the cell which is a measure of the relative nucleotide phosphate concentrations. High values of energy charge indicate higher relative triphosphate concentrations which leads to inhibition of catabolic pathways.[31]

The response in the presence of **ATP**, which is also contains a purine base, is extremely similar to that seen for **GTP**, (**Fig. S2**, ESI†). In contrast, **CTP**, which contains a pyrimidine base, showed a different optical response particularly in its absorption spectrum. A reduced red-shift in the absorption maximum of the PT block (**Fig. S3,** ESI†), along with a large decrease in the relative absorbance is observed on addition of **CTP**. Overall, the shift in the absorption band of the PT block and quenching of its emission suggests a specific interaction between the PT block and the nucleotides. This is most likely mediated by electrostatic interactions between the positively-charged pendent groups of the PT block and the negatively-charged phosphate groups on each nucleotide.

Table 1 Stern-Volmer constants, K_{SV}, and fitting parameters; f_a and K_s, for quenching of the PT emission of **PF2/6-*b*-P3TMAHT** in the presence of nucleotide phosphates for three quenching models (simple Sten-Volmer, Buried Fluorophore and Ionic Micelle). Unless otherwise indicated λ_{ex} = 380 nm.

	Simple Stern-Volmer Model[a]		Buried Fluorophore Model[b]		Ionic Micelle Model[c]	
Nucleotide	K_{SV} (λ_{ex} = 380 nm) ($\times 10^5$ M^{-1})[a]	K_{SV} (λ_{ex} = 430 nm) ($\times 10^5$ M^{-1})[a]	f_a	K_a ($\times 10^5$ M^{-1})	K_{SV} (M^{-1})	K_s (dm^3 mol^{-1} s^{-1}) ($\times 10^5$ M^{-1})
GTP	1.2 ± 0.3	1.1 ± 0.5	0.76±0.03	11.1 ± 0.6	2.44±0.06	3.3 ± 0.4
GDP	1.0 ± 0.1	0.8 ± 0.1	0.49±0.09	10.5 ± 2.0	1.79±0.05	2.5 ± 0.8
GMP	0.5 ± 0.1	0.5 ± 0.1	0.37±0.08	26.8 ± 5.0	0.49±0.10	1.3 ± 1.0
ATP	1.4 ± 0.2	2.5 ± 0.3	0.70±0.07	4.2 ± 0.6	2.02±0.2	1.3 ± 0.4
CTP	1.2 ± 0.3	1.0 ± 0.4	0.57±0.10	4.2 ± 3.0	1.43±0.10	2.4 ± 1.0

[a] Determined from a linear fit to the Stern-Volmer plots in Fig. 2 up to the charge compensation point, where $I_0/I = 1 + K_{SV}$[anion].
[b] Determined from a linear fit to the initial step portion of the plots for the Buried Fluorophore model, **Eqn. (4)**.
[c] Determined from a polynomial fit to the Ionic Micelle Model, **Eqn. (6)**.

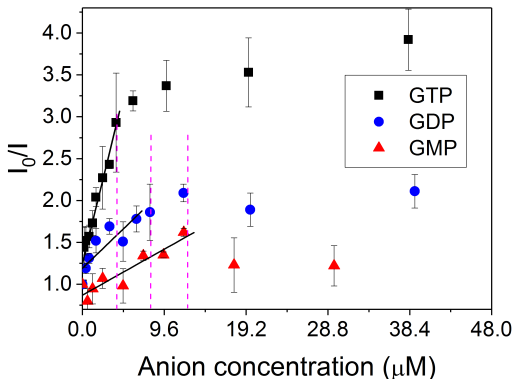

Figure 2 Stern-Volmer plots for quenching of PT emission on excitation of PF block (λ_{ex} = 380 nm) by **GTP** – black squares, **GDP** – blue circles and **GMP** – red triangles. The pink dash lines represent the charge equivalence point for the titration with each of the nucleotides (**GTP** - 40 μM, **GDP** - 80 μM, **GMP** - 120 μM). I_0 and I represent the emission intensity at 480 nm in the absence and presence of the anion, respectively.

We note that the studies here are performed in Millipore water rather than in buffered solution as the presence of small anions has previously been shown to affect the optical response of **PF2/6-*b*-P3TMAHT**[16] and we wished to isolate competitive interactions. Control experiments performed under the same conditions in Tris buffer resulted in similar but more dramatic quenching of the PT emission (ESI†, **Fig. S4**). However, in this buffered solution, a decrease in the PF emission was also noted suggesting either a change in FRET efficiency or screening effects brought about by the presence of the extra buffer ions, further encouraging the use of pure Millipore water solutions for this study. We note that the pH remained effectively unchanged during the course of the titrations in Millipore water (pH 7). As the pKa values for each of the phosphate protons are <6.5, each of the phosphate groups will be deprotonated at this pH.[32] The sensitivity of this ratiometric sensor lies in the μM region for each of the nucleotides examined. As the concentrations of nucleotide phosphates within the cell range from μM to mM[33] this platform is capable of detecting even small changes in these levels, thus providing important information about cellular energy status.

Mechanism of Quenching

The excited-state lifetime of **PF2/6-*b*-P3TMAHT** is unaffected on addition of the nucleotides investigated, suggesting that quenching occurs predominantly by a static quenching mode. This is reasonable considering an electrostatic interaction between the positively-charged PT blocks and the negatively-charged nucleotides. The occurrence of nucleotide-polymer binding was confirmed for **GTP** and the homopolymer **P3TMAHT** using isothermal calorimetry (see ESI† and **Fig. S5** for further details). Fitting to the calorimetric data, assuming a single set of equivalent binding sites, gave rise to a binding constant of 1.2 ± 0.5 × 10^6 M^{-1}. In addition, negative ΔH^0 (-10.3±0.9 kJ mol^{-1}) and positive ΔS^0 (0.08 kJ mol^{-1} K^{-1}) values were obtained, indicating that the binding of **GTP** to **P3TMAHT** is both enthalpically and entropically favourable. Stern-Volmer plots derived from the steady-state emission intensity data on addition of the guanosine-containing anions are shown as representative examples in **Fig. 2**. Each Stern-Volmer plot exhibits a steep linear portion that plateaus at the charge equivalence point. The Stern-Volmer constants, K_{SV}, determined from a linear fit to the initial steep portion of the plot up to the charge equivalence point are shown in **Table 1**.

However, the deviation from linearity at concentrations above the charge equivalence point may suggest that simple static quenching does not fully describe the quenching behaviour observed. One possibility for this deviation from linearity may be a change in the expected aggregate structure from that shown in **Scheme 1**. Previously, addition of negatively-charged surfactants to the homopolymer PT block, **P3TMAHT**, has been shown to causes a change from spherical polymer aggregates to cylindrical or sheet-like aggregates depending on the surfactant concentration.[17] However, if this were the case, spectral shifts and the appearance of vibrational structure would be expected, which we do not see here. Moreover, the K_{SV} values are similar for excitation *via* both the PF and PT blocks, as can be seen in **Table 1**, suggesting that the FRET efficiency is not altered dramatically, which would be expected if significant structural reorganisation had occurred upon analyte binding.

Another possibility is that a fraction of the PT sites are buried within the aggregate shell, thus effectively being inaccessible to the quencher in question. To assess this

possibility, the quenching data were fit to a model which describes a system in which a portion of the fluorophores are

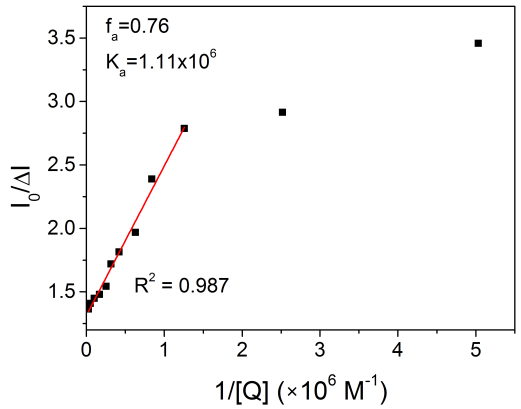

Figure 3. Linear fit to buried fluorophore model of modified Stern-Volmer plot for fluorescence quenching of **PF2/6-*b*-P3TMAHT** by **GTP** (λ_{ex} = 380 nm, λ_{em} = 480 nm).

buried within the aggregate structure and therefore inaccessible to the quencher.[34]

This leads to two separate populations of fluorophore, one of which is accessible (*a*) to quencher molecules and the other being inaccessible or buried (*b*). The total fluorescence in the absence of quencher (I_0) is given by:

$$I_0 = I_{0a} + I_{0b} \quad (1)$$

where the subscript '0' refers to the fluorescence intensity in the absence of quencher. The intensity of the available fraction, I_{0a}, decreases according to the Stern-Volmer relationship, while the buried fraction, I_{0b}, is not quenched and the resulting observed intensity is given by:

$$I = \frac{I_{0a}}{1 + K_a[Q]} + I_{0b} \quad (2)$$

where K_a is the quenching constant of the accessible fraction. Thus, the relative change in intensity is given by:

$$\Delta I = I_{0a}\left(\frac{K_a[Q]}{1 + K_a[Q]}\right) \quad (3)$$

This leads to the relationship:

$$\frac{I_0}{\Delta I} = \frac{1}{f_a K_a[Q]} + \frac{1}{f_a} \quad (4)$$

where f_a is the fraction of the initial fluorescence that is accessible to the quencher and is given by:

$$f_a = \frac{I_{0a}}{I_{0a} + I_{0b}} \quad (5)$$

Thus, a plot of $I_0/\Delta I$ *vs*. 1/[*Q*] should yield a straight line with an intercept of $1/f_a$ and a slope of $1/f_a K_a$.

On plotting $I_0/\Delta I$ *vs*. 1/[*Q*] for the quenching with each anion, the resulting data were found to not be completely linear, as can be seen for **GTP** in **Fig. 3**. As seen in the simple Stern-Volmer quenching model (**Fig. 2**), a steep linear portion was observed, followed by a deviation towards the *x*-axis. The fits to this buried fluorophore model give K_a constants in the range 4×10^5-3×10^6 M^{-1} and an accessible fraction of fluorophores that decreases with the number of phosphate groups on the anion (**Table 1**). These K_a constants are similar in magnitude to the K_{SV} values obtained through simple Stern-Volmer analysis.

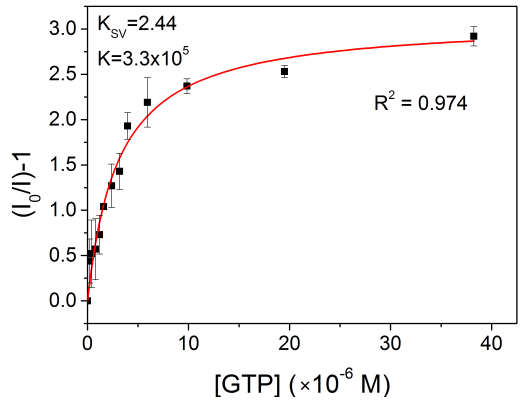

Figure 4. Fit to a multi-equilibrium model of modified Stern-Volmer plot for fluorescence quenching of **PF2/6-*b*-P3TMAHT** by **GTP** (λ_{ex} = 380 nm).

However, the lack of linearity in these plots indicates that a population of completely inaccessible fluorophores is not the cause of the observed deviation above the charge compensation point.

The core-shell aggregate structure observed for **PF2/6-*b*-P3TMAHT** in water[22] is rather similar to the formation of ionic micelles in solution. Recently, a model describing quenching in ionic micelles induced by counter-ions within the Stern layer has been found to accurately describe the quenching of **PF2/6-*b*-P3TMAHT** by smaller halide ions, which follow the order I^- >Br^- >Cl^-.[16] This model takes into account diffusion of a quencher held in the Stern layer into the core of an ionic micelle.[35] This is in contrast to the buried fluorophore model, in which the buried population is completely inaccessible to the quencher. This ionic micelle model was derived using a multi-equilibrium model[35] which leads to the modified Stern-Volmer relationship between the fluorescence intensity ratio and the quencher concentration:

$$\frac{I_0}{I} = 1 + \frac{\tau_0 k_q n K_s[Q]}{1 + K_s[Q]} = 1 + \frac{K_{sv} n K_s[Q]}{1 + K_s[Q]} \quad (6)$$

where *n* is the number of vacant sites, K_s is the association constant, τ_0 is the fluorescence lifetime, K_q is the quenching rate constant and K_{SV} is the Stern-Volmer constant.

The quenching data were plotted as (I_0/I)-1 *vs*. [*Q*] and fitted to the model in **Eqn. (6)**. This led to good fits to the quenching data for the nucleotides, see **Fig. 4** for **GTP** as a representative example (see **Fig. S6,** ESI† for the other systems). The K_{SV} values (**Table 1**) are all in the range of that reported for **PF2/6-*b*-P3TMAHT** when quenched by NaCl.[16] The good fits to the data and the agreement with literature for quenching by NaCl indicates that the quenching is adequately described by this multi-equilibrium model, in which the quenching is controlled by the nucleotides held in the Stern layer of a charged **PF2/6-*b*-P3TMAHT** aggregate that acts like an ionic micelle, with the PT blocks predominantly occupying the aggregate surface. The association constants extracted from fitting to this model are similar to those observed when fitting to the initial linear

portion of the Stern-Volmer plots (**Table 1**). This highlights the importance of the electrostatic interaction between the analyte and the CPE aggregate for the action of sensor. In the future, tailoring of this interaction by careful selection of the CPE charged group may extend the selectivity of this platform to other oppositely-charged analytes in aqueous media.

Electrochemical analysis

As the quenching observed in the system appears to be heavily dependent on electrostatic interactions between the PT block and the bioanalyte, electrochemical measurements were performed to investigate if electron transfer plays a role in the observed quenching. The cyclic voltammograms (CV) for **PF2/6-*b*-P3TMAHT** and the **P3TMAHT** homopolymer were measured (ESI†, **Fig. S7**). In forward bias **P3TMAHT** shows a reversible oxidation band at 1.03 V with a corresponding reduction peak at 0.92 V. These values are slightly higher than the first oxidation peak of the polymer backbone reported for similar polythiophenes containing oligo(oxyethylene) side chains in tetrahydrofuran (0.7 V),[36] but is slightly lower than that of poly(3-hexylthiophene) films in acetonitrile (1.3 V).[37] The CV of **P3TMAHT** also shows an irreversible reduction peak at -0.01 V, which is most likely to be associated with the charged species on the side chain, as it does not appear in the CV of the neutral homopolymer precursor with bromohexyl side chains, **P3BrHT** (ESI, **Fig S7c**). Introduction of the polyfluorene block to the **P3TMAHT** polymer shifts the observed oxidation peak to 0.88 V, with no associated reduction peak. To date there are very few reports of the solution phase electrochemistry of all-conjugated PF-PT block copolymers, however the observed redox properties for **PF2/6-*b*-P3TMAHT** are very similar to those reported previously for alternating fluorene-thiophene conjugated polymers which showed an oxidation peak ranging from 0.8 V to 0.94 V, depending on the side chain attached to the polythiophene repeat unit.[38] A large reduction peak is also observed in the CV of **PF2/6-*b*-P3TMAHT** at -0.33 V characteristic of a redox process associated with the ammonium side groups.[39] A polythiophene modified with a pyridinium side chain has previously been observed to exhibit a similarly pronounced reduction peak at a voltage characteristic of redox processes of the pyridinium.[37]

The redox potentials of the nucleobases (the heterocyclic components in the nucleotides) have previously been reported in organic solvents[40] and lie outside of the electrochemical window of water (-0.6 and 1.2 V, beyond which oxygen and hydrogen evolution occur).[41] Thus, the CVs of the nucleotides in water measured here are dominated by contributions from the phosphate components. As can be seen in **Fig. 5** for the guanosine-containing phosphates (see **Fig S8,** ESI† for CVs of **ATP** and **CTP**), each voltammogram contains several peaks attributed to the redox activity of the phosphate groups on each nucleotide according to their standard reduction potentials listed below:[42,43]

$$H_3PO_4 + 2H^+ + 2e^- \leftrightarrow H_3PO_3 + H_2O \qquad E^0 = -0.276\ V$$
$$H_3PO_3 + 2H^+ + 2e^- \leftrightarrow H_3PO_2 + H_2O \qquad E^0 = -0.499\ V$$

The possibility of photoinduced electron transfer between **PF2/6-P3TMAHT** and the nucleotides was investigated using the Rehm-Weller equation:[40]

$$\Delta G^0 = E_{ox}(D) - E_{red}(A) - E_{00} + C \qquad (7)$$

Table 2 Table of free energy change (ΔG^0) for electron transfer calculated using the Rehm-Weller equation from **PF2/6-*b*-P3TMAHT** to the nucleobase or the phosphate species.

Acceptor species	ΔG^0 (eV)
Nucleobase	
Guanosine	1.15
Adenosine	0.91
Cytidine	0.74
Phosphate	
RO-HPO_3	-0.79
RO- HPO_2- HPO_3	-0.99
RO- H_2PO_3	-1.11

where $E_{ox}(D)$ is the oxidation potential of the donor species, $E_{red}(A)$ is the reduction potential of the acceptor species, E_{00} is the energy of the zero-zero vibronic transition of the CPE and C is a solvent term that can be ignored in polar solvents.[44,45] The free energy change was estimated using the Rehm-Weller equation for both the situation where the polymer acts as the electron donor to the nucleobase and to the phosphate, the results of which are shown in **Table 2**. E_{00} was calculated from the overlap of the absorption and emission spectrum of **P3TMAHT** and found to be 2.29 eV.

The negative values for ΔG^0 shown in **Table 2** suggest that phot-induced electron transfer occurs from the CPE to the phosphates of the nucleotides. This agrees well with the quenching data which depend on the number of phosphate groups and follow the trend **GTP**>**GDP**>**GMP**. The response in the presence of adenosine triphosphate, which is also a purine-based nucleotide is very similar to that seen for **GTP**. The slight difference observed in the optical response for **CTP,** which also contains three phosphate groups, may be rationalised rather by the size of the pyrimidine nucleobase. The smaller nucleobase may induce less change in the aggregation state of the CPE on electrostatic binding, leading to the lack of red shift noted in the UV/Vis absorption spectra and slightly reduced quenching observed in the PL spectra. This suggests that the response brought about *via* photoinduced electron transfer may be coupled to any change brought about by a transformation in the aggregate structure.

Conclusions

The optical response of the cationic all-conjugated diblock copolymer **PF2/6-*b*-P3TMAHT** was mapped in the presence of the biologically-important nucleotide phosphates **GTP**, **GDP**, **GMP**, **ATP** and **CTP** at biologically relevant concentrations. Previous studies on **PF2/6-*b*-P3TMAHT** in water have shown that it adopts an aggregate structure with a PF-rich core surrounded by PT blocks. Addition of the purine-based nucleotide phosphates examined here leads to a red shift in the

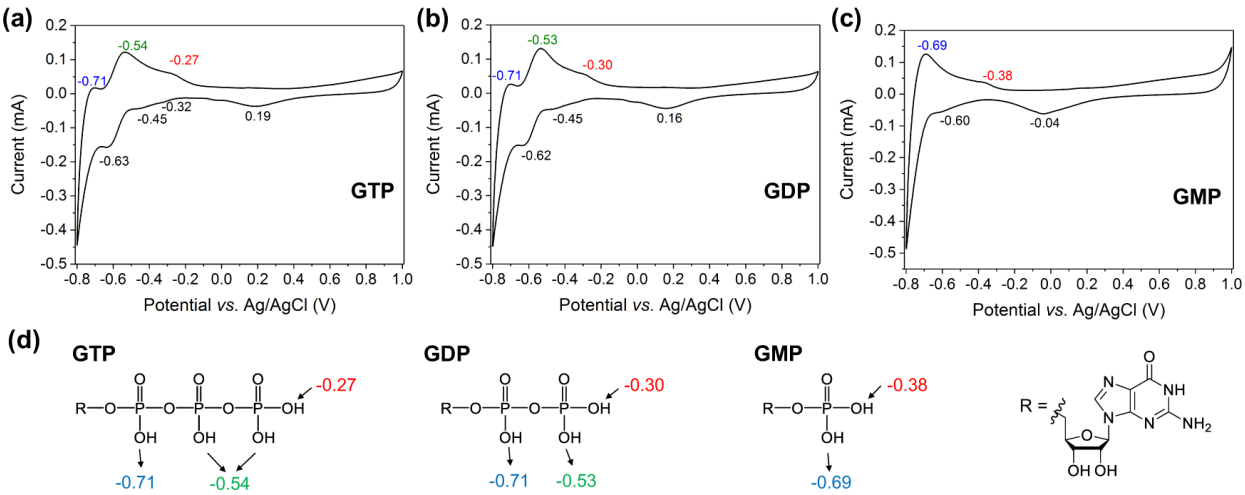

Figure 5. Cyclic voltammograms for (**a**) **GTP**, (**b**) **GDP** and (**c**) **GMP** in H_2O at 50 mV s^{-1} scan rate using Pt as the working and counter electrode, Ag/AgCl as reference electrode and KCl (0.1 M) as the supporting electrolyte.(**d**) Assignment of CV Peaks for each reduction process depending on the number of phosphates present on the nucleotide. **GTP**, **GDP** and **GMP**.

UV/Vis absorption maximum of the PT block which is dependent on the number of phosphate groups, *e.g.* **GTP**>**GDP**>**GMP**. In contrast, addition of the pyrimidine-based nucleotide **CTP** gives rise to a decrease in the PT absorbance. The selective response of only the PT block suggests a specific electrostatic interaction operates between the negatively-charged bioanalyte and the cationic PT block. On excitation into the PF block (λ_{ex} = 380 nm), partial FRET to the PT block gives rise to emission from both blocks. The PT emission is quenched in the presence of all of the nucleotide phosphates examined with the magnitude of the quenching being dependent on the number of phosphates attached to the nucleobase. The PF emission is unaffected by the presence of the bioanalyte, supporting a core-shell type structure in aqueous solution, in which the PF blocks are less accessible. This provides an internal reference, creating a ratiometric sensor platform.

Modelling of this quenching behaviour suggests that the process is not simply described by normal static or dynamic processes, but is in fact better described by quenching of the fluorophores by counter ions held with the Stern layer of the charged aggregate. Electrochemical studies indicate that photo-induced electron transfer occurs from the PT block of **PF2/6-*b*-P3TMAHT** to the phosphate groups of the nucleotides. The differences observed between the purine and pyrimidine nucleobases suggest that this CPE may be developed further as a platform sensor technology to differentiate between redox active species of different sizes, coupling the quenching brought about by photoinduced electron transfer with the possibility of varying the aggregation state depending on the size and shape of the analyte.

Experimental

Materials

Poly[9,9-bis(2-ethylhexyl)fluorene]-*b*-poly[3-(6-triethylammoniumhexyl)thiophene] bromide (**PF2/6-*b*-P3TMAHT**) was synthesised as previously reported[22,24] with a number-averaged molecular weight, M_n, of 28,250 g mol^{-1} (m = 37, n = 46) by gel permeation chromatography (GPC), measured for the polymer precursor with bromohexyl side chains. We note that direct molecular weight measurement of the cationic polymer is not possible due to strong interaction of the CPE with the GPC column. Complete conversion of the bromohexyl precursor to the quarternary ammonium group was confirmed, within detection limits, by ^{1}H NMR spectroscopy. Potassium chloride (≥99%), guanosine triphosphate sodium salt hydrate (≥95%), guanosine diphosphate sodium salt hydrate (≥96%), guanosine monophosphate sodium salt hydrate (≥99%), cytidine triphosphate disodium salt (≥95%) and adenosine triphosphate disodium salt (≥99%) were purchased from Sigma Aldrich and used as received.

Instrumentation

UV/Vis absorption spectra were recorded on a Shimadzu UV2401 PC UV/Vis scanning spectrometer with slit width of 1 nm. Photoluminescence measurements were performed using a Fluorolog-3 spectrophotometer (Horiba Jobin Yvon). Emission and excitation slit widths were maintained at 2.0 nm. Emission and excitation spectra were corrected for the wavelength response of the system and the intensity of the lamp profile over the excitation range, respectively, using correction factors supplied by the manufacturer.

ITC experiments were performed using a MicroCal VP-ITC instrument (MicroCal Inc., Northampton, MA) interfaced with a computer equipped with VP-2000 viewer instrument control software. ITC data were analysed with Origin 7.0 software. In ITC experiments 2 µl of a 500 µM guanosine triphosphate (**GTP**) solution was injected every 180 s for a total of 15 injections into a solution of **P3TMAHT** in the calorimeter cell at 30 µM. The

observed heat for each injection (peak) was measured by area integration of the power peak with respect to time. ITC data were fitted according to a standard model that assumes a single set of equivalent binding sites (see ESI for further details).
All electrochemical experiments were undertaken in a standard three-electrode cell. The working and counter electrodes were Pt wires, while an Ag/AgCl electrode was employed as the reference electrode. Cyclic voltammograms were measured using 0.1 M potassium chloride (KCl) as the supporting electrolyte. The electrochemical measurements were performed using a high performance digital potentiostat (CH model 1760 D Bi-potentiostat system monitored using CH1760D electrochemical workstation beta software). All solutions were degassed for 15 min before the analysis to eliminate any dissolved oxygen present in the electrolyte.

Conflicts of Interest

There are no conflicts of interest to declare.

Acknowledgements

The authors thank Dr. Colm Delaney for assistance with initial electrochemical analysis. This work was supported in part by Science Foundation Ireland under Grant No 12/IP/1608. N. W.-F. thanks the Irish Research Council for a Government of Ireland postgraduate studentship.

Notes and references

1. Y. Liu, V. V. Duzhko, Z. A. Page, T. Emrick and T. P. Russell, *Acc. Chem. Res.*, 2016, **49,** 2478.
2. C. Duan, K. Zhang, C. Zhong, F. Huang and Y. Cao, *Chem. Soc. Rev.*, 2013, **42,** 9071.
3. Z. Chen, P. Wu, R. Cong, N. Xu, Y. Tan, C. Tan and Y. Jiang, *ACS Appl. Mater. Interfaces*, 2016, **8,** 3567.
4. G. Feng, J. Liang and B. Liu, *Macromol. Rapid Commun.*, 2013, **34,** 705.
5. S. Rochat and T. M. Swager, *Angew. Chem. Int. Ed.*, 2014, **53,** 9792.
6. H. Jiang, P. Taranekar, J. R. Reynolds and K. S. Schanze, *Angew. Chem. Int. Ed.*, 2009, **48,** 4300.
7. Z. Liu, H.-L. Wang and M. Cotlet, *Chem. Mater.*, 2014, **26,** 2900.
8. M. Zhao, L. Yang, R. Zhang, J. Dong, H. Dong, Y. Wen, X. Zhan, G. Wang, Y. Lu and G. Wang, *Polymer*, 2013, **54,** 297.
9. D. Wu and K. S. Schanze, *ACS Appl. Mater. Interfaces*, 2014, **6,** 7643.
10. J. E. Houston, M. Kraft, U. Scherf and R. C. Evans, *Phys. Chem. Chem. Phys.,* 2016**, 18**, 12423.
11. Y. Liu, K. Ogawa and K. S. Schanze, *Anal. Chem.*, 2008, **80,** 150.
12. S. Das, P. Routh, R. Ghosh, D. P. Chatterjee, D. and A. K. Nandi, *Polym. Int.*, 2017, **66,** 623.
13. J. E. Houston, M. Kraft, I. Mooney, A. E. Terry, U. Scherf and R. C. Evans*, *Langmuir*, 2016, **32**, 8141.
14. Z. Yao, X. Feng, W. Hong, C. Li, and G. A. Shi, *Chem. Commun.*, 2009, **0,** 4696.
15. J. M. Berg, J. L. Tymocko and L. Stryer, *Biochemistry*, W. H. Freeman and Company, 2012, pp. 446-449.
16. S. M. Fonseca, R. P. Galvão, H. D. Burrows, A. Gutacker, U. Scherf and G. C. Bazan, *Macromol. Rapid Commun.*, 2013, **34,** 717.
17. R. C. Evans, M. Knaapila, N. Willis-Fox, M. Kraft, A. Terry, H. D. Burrows and U. Scherf, *Langmuir*, 2012, **28,** 12348.
18. A. Yassar, L. Miozzo, R. Gironda and G. Horowitz, *Prog. Polym. Sci.*, 2013, **38,** 791.
19. U. Scherf, A. Gutacker, and N. Koenen, *Acc. Chem. Res.*, 2008, **41,** 1086.
20. G. Tu, H. Li, M. Forster, F. Heiderhoff, L. J. Balk, R. Sigel and U. Scherf, *Small*, 2007, **3,** 1001.
21. U. Scherf, R. C. Evans, A. Gutacker and G. C. Bazan, *Conjugated Polyelectrolytes: Fundamentals and Applications*, Wiley-VCH Verlag GmbH & Co, 2012, Eds. B. Liu & G. C. Bazan, pp. 65-89.
22. A. Gutacker, N. Koenen, U. Scherf, S. Adamczyk, J. Pina, S. M. Fonseca, A. J. M. Valente, R. C. Evans, J. Sexias de Melo, H. D. Burrows and M. Knaapila, *Polymer*, 2010, **51,** 1898.
23. A. Gutacker, S. Adamczyk, A. Helfer, L. E. Garner, R. C. Evans, S. M. Fonseca, M. Knaapila, G. C. Bazan, H. D. Burrows and U. Scherf, *J. Mater. Chem.*, 2010, **20,** 1423.
24. M. Knaapila, R. C. Evans, A. Gutacker, V. M. Garamuz, M. Torkkeli, S. Adamczyk, M. Forster, U. Scherf and H. D. Burrows, *Langmuir*, 2010, **26,** 5056.
25. M. Knaapila, T. Costa, V. M. Garamus, M. Kraft, M. Drechsler, U. Scherf and H. D. Burrows, *J. Phys. Chem. B*, 2015, **119,** 3231.
26. J. M. Berg, J. L. Tymocko and L. Stryer, *Biochemistry*, W. H. Freeman and Company, 2012, pp. 114-116.
27. J. M. Berg, J. L. Tymocko and L. Stryer, *Biochemistry*, W. H. Freeman and Company, 2012, pp. 108-111.
28. R. H. Garrett and C. M. Grisham, *Biochemistry*, Brooks/Cole, 2016, pp. 290.
29. R. Yang, A. Garcia, D. Korystov, A. Mikhailovsky, G. C. Bazan and T.-Q. Nguyen, *J. Am. Chem. Soc.*, 2006, **128,** 16532.
30. J. R. Knowles, *Annu. Rev. Biochem.*, 1980, **49,** 877.
31. D. G. Hardie and S. A. Hawley, *BioEssays, 2001,* **23,** 1112.
32. P. Kaczmarek, W. Szczepanik and M. Jeżowska-Bojczuk, *Dalton Trans.*, 2005, **0,** 3653.
33. T. W. Traut, *Mol. Cell. Biochem.*, 1994, **140,** 1.
34. J. R. Lakowicz, *Principles of Fluorescence Spectroscopy*, Springer, 2006, pp.289.
35. H. D. Burrows, S. J. Formosinho, M. F. J. R. Paiva and E. J. Rasburn, *J. Chem. Soc. Faraday Trans. 2*, 1980, **76,** 685.
36. R. van Beek, L. W. Jenneskens, A. N. Zdravkova, J. P. J. M. van der Eerden and C. A. Walree, *Macromol. Chem. Phys.*, 2005, **206**, 1006.
37. Y. Li, K. Kamata, S. Asaoka, T. Yamagishi and T. Iyoda, *Org. Biomol. Chem.*, 2003, **1**, 1779.
38. B. Zhao, D. Liu, L. Peng, H. Li, P. Shen, N. Xiang, Y. Liu and S. Tan, *Euro. Poly. J.*, 2009, **45**, 2079.
39. *Handbook of Property Estimation Methods for Chemicals: Environmental Health Sciences,* CRC Press, 2000, Ed. D. Mackay and R. S. Boethling.
40. C. A. M. Seidel, A. Schulz and M. H. M. Sauer, *J. Phys. Chem.*, 1996, **100,** 5541.
41. T. Fuchigami, S. Inagi and M. Atobe, *Fundamentals and Applications of Organic Electrochemistry*, John Wiley & Sons Ltd, 2014, pp. 217–222.
42. *CRC Handbook of Chemistry and Physics*, CRC Press, 2012, Ed. W. M. Haynes.
43. *CRC Handbook of Chemistry and Physics,* CRC Press, 2006, Ed. D. R. Lide.

44. T. Heinlein, J.-P. Knemeyer, O. Piestert and M. Sauer, *J. Phys. Chem. B*, 2003, **107,** 7957.
45. M. Torimura, S. Kurata, K. Yamada, T. Yokomaku, Y. Kamagata, T. Kanagawa and R. Kurane, *Anal. Sci.*, 2001, **17,** 155.